Available online at www.sciencedirect.com

ScienceDirect

Nuclear Physics B 897 (2015) 77–86

NUCLEAR PHYSICS B

www.elsevier.com/locate/nuclphysb

The effective QCD phase diagram and the critical end point

Alejandro Ayala [a,b], Adnan Bashir [c], J.J. Cobos-Martínez [c,*], Saúl Hernández-Ortiz [c], Alfredo Raya [c]

[a] *Instituto de Ciencias Nucleares, Universidad Nacional Autónoma de México, Apartado Postal 70-543, México Distrito Federal 04510, Mexico*

[b] *Centre for Theoretical and Mathematical Physics, and Department of Physics, University of Cape Town, Rondebosch 7700, South Africa*

[c] *Instituto de Física y Matemáticas, Universidad Michoacana de San Nicolás de Hidalgo, Edificio C-3, Ciudad Universitaria, Morelia, Michoacán 58040, Mexico*

Received 2 December 2014; received in revised form 24 April 2015; accepted 12 May 2015

Available online 14 May 2015

Editor: Hong-Jian He

Abstract

We study the QCD phase diagram on the temperature T and quark chemical potential μ plane, modeling the strong interactions with the linear sigma model coupled to quarks. The phase transition line is found from the effective potential at finite T and μ taking into account the plasma screening effects. We find the location of the critical end point (CEP) to be $(\mu^{\rm CEP}/T_c, T^{\rm CEP}/T_c) \sim (1.2, 0.8)$, where T_c is the (pseudo)critical temperature for the crossover phase transition at vanishing μ. This location lies within the region found by lattice inspired calculations. The results show that in the linear sigma model, the CEP's location in the phase diagram is expectedly determined solely through chiral symmetry breaking. The same is likely to be true for all other models which do not exhibit confinement, provided the proper treatment of the plasma infrared properties for the description of chiral symmetry restoration is implemented. Similarly, we also expect these corrections to be substantially relevant in the QCD phase diagram.

* Corresponding author.
E-mail address: javiercobos@ifm.umich.mx (J.J. Cobos-Martínez).

http://dx.doi.org/10.1016/j.nuclphysb.2015.05.014

The different phases in which matter, made up of quarks and gluons, arranges itself depends, as for any other substance, on the temperature and density, or equivalently, on the temperature and chemical potentials. Under the assumptions of beta decay equilibrium and charge neutrality, the representation of the QCD phase diagram is two dimensional. This is customary plotted with the light-quark chemical potential μ as the horizontal variable and the temperature T as the vertical one. μ is related to the baryon chemical potential μ_B by $\mu_B = 3\mu$.

Most of our knowledge of the phase diagram is restricted to the $\mu = 0$ axis. The phase diagram is, by and large, unknown. For physical quark masses and $\mu = 0$, lattice calculations have shown [1] that the change from the low temperature phase, where the degrees of freedom are hadrons, to the high temperature phase described by quarks and gluons is an analytic crossover. The phase transition has a dual nature: on the one hand, the color-singlet hadrons break up leading to deconfined quarks and gluons; this is dubbed as the *deconfinement phase transition*. On the other hand, the dynamically generated component of quark masses within hadrons vanishes; this is referred to as *chiral symmetry restoration*.

Lattice calculations have provided values for the crossover (pseudo)critical temperature T_c for $\mu = 0$ and $2 + 1$ quark flavors using different types of improved rooted staggered fermions [2]. The MILC Collaboration [3] obtained $T_c = 169(12)(4)$ MeV. The RBC-Bielefeld Collaboration [4] reported $T_c = 192(7)(4)$ MeV. The Wuppertal-Budapest Collaboration [5] has consistently obtained smaller values, the latest being $T_c = 147(2)(3)$ MeV. The HotQCD Collaboration has computed $T_c = 154(9)$ MeV [6] and more recently $T_c = 155(1)(8)$ MeV [7]. The differences could perhaps be attributed to different lattice spacings.

The picture presented by lattice QCD for $T \geq 0$, $\mu = 0$ cannot be easily extended to the case $\mu \neq 0$, the reason being that standard Monte Carlo simulations can only be applied to the case where either $\mu = 0$ or it is purely imaginary. Simulations with $\mu \neq 0$ are hindered by the *sign problem*, see, for example, [8], though some mathematical extensions of lattice techniques [9] can probe this region. Schwinger–Dyson equation techniques can also be employed to explore all region of the phase space [10].

On the other hand, a number of different model approaches indicate that the transition along the μ axis, at $T = 0$, is strongly first order [11]. Since the first-order line originating at $T = 0$ cannot end at the $\mu = 0$ axis which corresponds to the starting point of the cross-over line, it must terminate somewhere in the middle of the phase diagram. This point is generally referred to as the critical end point (CEP). The location and observation of the CEP continue to be at the center of efforts to understand the properties of strongly interacting matter under extreme conditions. The mathematical extensions of lattice techniques place the CEP in the region $(\mu^{\text{CEP}}/T_c, T^{\text{CEP}}/T_c) \sim (1.0\text{–}1.4, 0.9\text{–}0.95)$ [12].

In the first reference of [10], it is argued that the theoretical location of the CEP depends on the size of the confining length scale used to describe strongly interacting matter at finite density/temperature. This argument is supported by the observation that the models which do not account for this scale [13–16] produce either a CEP closer to the μ axis (μ^{CEP}/T_c and T^{CEP}/T_c larger and smaller, respectively) or a lower T_c [17] than the lattice based approaches or the ones which consider a finite confining length scale. Given the dual nature of the QCD phase transition, it is interesting to explore whether there are other features in models which have access only to the chiral symmetry restoration facet of QCD that, when properly accounted for, produce the CEP's location more in line with lattice inspired results.

An important clue is provided by the behavior of the critical temperature as a function of an applied magnetic field. Lattice calculations have found that this temperature decreases when the field strength increases [18–20]. It has been recently shown that this phenomenon, dubbed *in-*

verse magnetic catalysis, is not due exclusively to confinement but instead that chiral symmetry restoration plays an important role. This result is born out of the decrease of the coupling constant with increasing field strength and is obtained within effective models that do not have confinement such as the Abelian Higgs model or the linear sigma model with quarks. The novel feature implemented in these calculations is the handling of the screening properties of the plasma, which effectively makes the treatment go beyond the mean field approximation [21,22]. The importance of accounting for screening in plasmas where massless bosons appear has been pointed out since the pioneering work in Ref. [23] and implemented in the context of the Standard Model to study the electroweak phase transition [24]. Screening is also important to obtain a decrease of the coupling constant with the magnetic field strength in QCD in the Hard Thermal Loop approximation [25].

In this work we explore the consequences of the proper handling of the plasma screening properties in the description of the effective QCD phase diagram within the linear sigma model with quarks [26]. We argue that it is the adequate description of the plasma screening properties for the chiral symmetry breaking within the model which determines the CEP's location. Since the linear sigma model does not exhibit confinement, one could think that the present calculation refers to finding the location of the CEP associated with chiral symmetry restoration. However, although at present there are no theoretical calculations, stemming from first principles, that prove the coincidence of chiral symmetry restoration and deconfinement transitions, there is nevertheless evidence that this may be the case, at least for not too high values of the chemical potential. The evidence is provided by lattice studies for $\mu = 0$ and $T \neq 0$. Their computation of the Polyakov loop and the light quark condensate susceptibilities indicates that the transition regions coincide. Calculations based on solutions of Schwinger–Dyson equations are in agreement with this statement as well [27]. Therefore, even though strictly speaking our approach can only access chiral symmetry restoration, we emphasize that both transitions can also take place around the same region in the (μ, T) plane and therefore that, to have access to the critical values for either transition, it may be enough to only look at one of the transition aspects. We find that for certain values of the model parameters, obtained from physical constraints, the CEP's location agrees with lattice inspired calculations.

We start from the linear sigma model coupled to quarks. It is given by the Lagrangian density

$$\begin{aligned}\mathcal{L} &= \frac{1}{2}(\partial_\mu \sigma)^2 + \frac{1}{2}(\partial_\mu \vec{\pi})^2 + \frac{a^2}{2}(\sigma^2 + \vec{\pi}^2) \\ &\quad - \frac{\lambda}{4}(\sigma^2 + \vec{\pi}^2)^2 + i\bar{\psi}\gamma^\mu \partial_\mu \psi \\ &\quad - g\bar{\psi}(\sigma + i\gamma_5 \vec{\tau}\cdot\vec{\pi})\psi, \end{aligned} \tag{1}$$

where ψ is an SU(2) isospin doublet, $\vec{\pi} = (\pi_1, \pi_2, \pi_3)$ is an isospin triplet and σ is an isospin singlet. The neutral pion is taken as the third component of the pion isovector, $\pi^0 = \pi_3$ and the charged pions as $\pi_\pm = (\pi_1 \mp i\pi_2)/2$. The squared mass parameter a^2 and the self-coupling λ and g are taken to be positive.

To allow for the spontaneous breaking of symmetry, we let the σ field develop a vacuum expectation value v

$$\sigma \to \sigma + v, \tag{2}$$

which can later be taken as the order parameter of the theory. After this shift, the Lagrangian density can be rewritten as

$$\mathcal{L} = -\frac{1}{2}\sigma\,\partial_\mu\partial^\mu\sigma - \frac{1}{2}\left(3\lambda v^2 - a^2\right)\sigma^2 - \frac{1}{2}\vec{\pi}\,\partial_\mu\partial^\mu\vec{\pi} - \frac{1}{2}\left(\lambda v^2 - a^2\right)\vec{\pi}^2 + \frac{a^2}{2}v^2 - \frac{\lambda}{4}v^4 + i\bar{\psi}\gamma^\mu\partial_\mu\psi - g v\bar{\psi}\psi + \mathcal{L}_I^b + \mathcal{L}_I^f, \tag{3}$$

where $\mathcal{L}_I^b$ and $\mathcal{L}_I^f$ are given by

$$\mathcal{L}_I^b = -\frac{\lambda}{4}\Big[(\sigma^2 + (\pi^0)^2)^2 + 4\pi^+\pi^-(\sigma^2 + (\pi^0)^2 + \pi^+\pi^-)\Big],$$
$$\mathcal{L}_I^f = -g\bar{\psi}(\sigma + i\gamma_5\vec{\tau}\cdot\vec{\pi})\psi, \tag{4}$$

and describe the interactions among the fields σ, $\vec{\pi}$ and ψ, after symmetry breaking. From Eq. (3) we see that the σ, the three pions and the quarks have masses

$$m_\sigma^2 = 3\lambda v^2 - a^2,$$
$$m_\pi^2 = \lambda v^2 - a^2,$$
$$m_f = g v, \tag{5}$$

respectively.

The one-loop effective potential for the linear sigma model with quarks including the plasma screening properties encoded in the ring diagrams contribution has been calculated in detail for zero chemical potential in previous works [28,29]. It is given by

$$V^{(\mathrm{eff})} = -\frac{a^2}{2}v^2 + \frac{\lambda}{4}v^4 + \sum_{i=\sigma,\vec{\pi}}\left\{\frac{m_i^4}{64\pi^2}\left[\ln\left(\frac{(4\pi T)^2}{2a^2}\right) - 2\gamma_E + 1\right] - \frac{\pi^2 T^4}{90} + \frac{m_i^2 T^2}{24} - \frac{T}{12\pi}(m_i^2 + \Pi)^{3/2}\right\} - N_c\sum_{f=u,d}\left\{\frac{m_f^4}{16\pi^2}\left[\ln\left(\frac{(\pi T)^2}{2a^2}\right) - 2\gamma_E + 1\right] - \frac{m_f^2 T^2}{12} + \frac{7\pi^2 T^4}{180}\right\}, \tag{6}$$

where $\Pi = \frac{\lambda T^2}{2} + \frac{N_f N_c g^2 T^2}{6}$ is the self-energy for any of the bosons. The analysis in Refs. [28,29] shows that the inclusion of the ring diagrams renders the effective potential stable.

When the chemical potential is non-vanishing, the calculation of the effective potential is more complicated. Though the boson contribution remains the same, the fermion contribution has to be modified due to the chemical potential. The modification enters the calculation in two ways: indirectly into the boson self-energy and directly from its contribution to the effective potential. We compute explicitly the latter below.

To one-loop order the fermion contribution to the effective potential in the imaginary time formalism of thermal field theory is given by [28]

$$V_f = -\frac{2}{\beta}\int\frac{\mathrm{d}^3k}{(2\pi)^3}\left[\beta\omega + \ln\left(1 + e^{-\beta(\omega-\mu)}\right) + \ln\left(1 + e^{-\beta(\omega+\mu)}\right)\right], \tag{7}$$

where $\beta = T^{-1}$ and $\omega = (\vec{k}^2 + m_f^2)^{1/2}$, and the sum over the fermion Matsubara frequencies has been performed. The first term in Eq. (7) corresponds to the vacuum contribution whereas

the second and third ones are the matter contributions. Note that the matter contribution is made out of separate quark and antiquark pieces due to the finite chemical potential. The vacuum contribution is well-known [28] and can be expressed, after mass renormalization as a function of the renormalization scale $\tilde{\mu}$. For the evaluation of the medium's contribution in Eq. (7) we will adapt the technique from Ref. [23] to the present case.

The main idea of this method is to produce a second-order differential equation in y^2, where $y = m_f/T$, valid at high temperature with m_f as the smallest of all scales, for the finite temperature part of the potential, which we will denote by $\tilde{V}_f$, given in Eq. (7) with appropriate boundary conditions at $y = 0$, where the integrals can be analytically evaluated. The expression for the effective potential is obtained by integrating this differential equation and using the given boundary conditions. The second-order differential equation satisfied by $\tilde{V}_f$ is

$$\frac{d^2\tilde{V}_f}{dy^4} = \frac{1}{8\pi^2\beta^4}\left[\ln\left(\frac{y^2}{(4\pi)^2}\right) - \psi^0\left(\frac{1}{2}+\frac{iz}{2\pi}\right) - \psi^0\left(\frac{1}{2}-\frac{iz}{2\pi}\right)\right], \tag{8}$$

where $\psi^0(x)$ is the digamma function. The boundary conditions are

$$\begin{aligned}\tilde{V}_f\big|_{y^2=0} &= \frac{2}{\pi^2\beta^4}\left[Li_4(-e^z) + Li_4(-e^{-z})\right]\\ \left.\frac{d\tilde{V}_f}{dy^2}\right|_{y^2=0} &= \frac{-1}{2\pi^2\beta^4}\left[Li_2(-e^z) + Li_2(-e^{-z})\right],\end{aligned} \tag{9}$$

where $Li_n(x)$ is the polylogarithm function of order n.

The boundary conditions (9) fix the two integration constants needed to determine $\tilde{V}_f(y,z)$. The solution of Eq. (8) that satisfies the boundary conditions (9) is given by

$$\begin{aligned}\tilde{V}_f = -\frac{1}{16\pi^2\beta^4}\Bigg\{&-y^4\ln\left(\frac{y^4}{(4\pi)^2}\right)\\ &+ y^4\left[\frac{3}{2} + \psi^0\left(\frac{1}{2}+\frac{iz}{2\pi}\right) + \psi^0\left(\frac{1}{2}-\frac{iz}{2\pi}\right)\right]\\ &+ 8y^2\left[Li_2(-e^z) + Li_2(-e^{-z})\right]\\ &- 32\left[Li_4(-e^z) + Li_4(-e^{-z})\right]\Bigg\}.\end{aligned} \tag{10}$$

Combining the vacuum contribution after mass renormalization with the finite temperature part and recalling that $y = m_f/T$ and $z = \mu/T$ we finally have

$$\begin{aligned}\tilde{V}_f = -\frac{1}{16\pi^2}\Bigg\{&m_f^4\left[\ln\left(\frac{(4\pi T)^2}{2\tilde{\mu}^2}\right) + \psi^0\left(\frac{1}{2}+\frac{i\mu}{2\pi T}\right) + \psi^0\left(\frac{1}{2}-\frac{i\mu}{2\pi T}\right)\right]\\ &+ 8m^2T^2\left[Li_2(-e^{\mu/T}) + Li_2(-e^{-\mu/T})\right]\\ &- 32T^4\left[Li_4(-e^{\mu/T}) + Li_4(-e^{-\mu/T})\right]\Bigg\}.\end{aligned} \tag{11}$$

It can also be shown that the boson self-energy Π, computed for a finite chemical potential and in the limit where the masses are small compared to T, is given by

$$\Pi = \frac{\lambda T^2}{2} - \frac{N_f N_c g^2 T^2}{\pi^2}\left[Li_2(-e^{\mu/T}) + Li_2(-e^{-\mu/T})\right] \tag{12}$$

where $N_f = 2$ and $N_c = 3$ are the numbers of light flavors and colors, respectively.

Choosing the renormalization scale as $\tilde{\mu} = e^{-1/2}a$, the effective potential up to the ring diagrams contribution for a finite chemical potential and in the limit where the masses are small compared to T is then given by

$$\begin{aligned} V^{(\text{eff})} = & -\frac{a^2}{2}v^2 + \frac{\lambda}{4}v^4 + \sum_{i=\sigma,\vec{\pi}}\left\{\frac{m_i^4}{64\pi^2}\left[\ln\left(\frac{(4\pi T)^2}{2a^2}\right) - 2\gamma_E + 1\right]\right. \\ & \left. - \frac{\pi^2 T^4}{90} + \frac{m_i^2 T^2}{24} - \frac{T}{12\pi}(m_i^2 + \Pi)^{3/2}\right\} \\ & - \frac{N_c}{16\pi^2}\sum_{f=u,d}\left\{m_f^4\left[\ln\left(\frac{(4\pi T)^2}{2a^2}\right) + 1\right.\right. \\ & \left. + \psi^0\left(\frac{1}{2} + \frac{i\mu}{2\pi T}\right) + \psi^0\left(\frac{1}{2} - \frac{i\mu}{2\pi T}\right)\right] \\ & + 8\, m_f^2 T^2\left[Li_2(-e^{\mu/T}) + Li_2(-e^{-\mu/T})\right] \\ & \left. - 32\, T^4\left[Li_4(-e^{\mu/T}) + Li_4(-e^{-\mu/T})\right]\right\}. \end{aligned} \tag{13}$$

In the limit when $\mu \to 0$, Eq. (13) becomes Eq. (6). In the same limit, Eq. (12) reduces to the well-known expression for the self-energy at high temperature [22].

Note that the self-energy provides the screening to render the effective potential in Eq. (13) stable. Should this self-energy be absent, the term $(m_i^2 + \Pi)^{3/2}$ would instead be $(m_i^2)^{3/2}$, which becomes imaginary when for certain values of v, m_i^2 becomes negative [see Eqs. (5)]. This term is obtained from considering the resummation of the ring diagrams and therefore Eq. (13) represents the effective potential computed beyond the mean field approximation that accounts for the leading screening effects at high temperature.

In order to find the values of the parameters λ, g and a appropriate for the description of the phase transition, we note that when considering the thermal effects the boson masses are modified since they acquire a thermal component. For $\mu = 0$ they become

$$\begin{aligned} m_\sigma^2(T) &= 3\lambda v^2 - a^2 + \frac{\lambda T^2}{2} + \frac{N_f N_c g^2 T^2}{6} \\ m_\pi^2(T) &= \lambda v^2 - a^2 + \frac{\lambda T^2}{2} + \frac{N_f N_c g^2 T^2}{6}. \end{aligned} \tag{14}$$

At the phase transition, the curvature of the effective potential vanishes for $v = 0$. Since the boson thermal masses are proportional to this curvature, these also vanish at $v = 0$. From any of Eqs. (14), we obtain a relation between the model parameters at T_c given by

$$a = T_c\sqrt{\frac{\lambda}{2} + \frac{N_f N_c g^2}{6}}. \tag{15}$$

Furthermore, we can fix the value of a by noting from Eqs. (5) that the vacuum boson masses satisfy

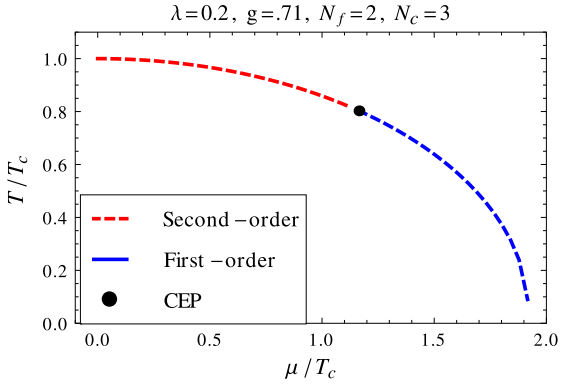

Fig. 1. Effective QCD phase diagram computed for $\lambda = 0.2$ and $g = 0.71$ obtained by considering $m_\sigma^{\rm vac} = 300$ MeV. For small values of μ the phase transition is of second order. The order of the transition changes to first order for larger values of μ. The CEP is located at $(\mu^{\rm CEP}/T_c, T^{\rm CEP}/T_c) \sim (1.2, 0.8)$.

$$a = \sqrt{\frac{m_\sigma^2 - 3m_\pi^2}{2}}. \tag{16}$$

Since in our scheme we consider two-flavor massless quarks in the chiral limit, we take $T_c \simeq 170$ MeV [30] which is slightly larger than T_c obtained in $N_f = 2+1$ lattice simulations. Also, in order to allow for a crossover phase transition for $\mu = 0$ (which in our description corresponds to a second-order transition) with g, $\lambda \sim 1$ we need that $g^2 > \lambda$. To justify the perturbative expansion we need to look for coupling constant values not too large. Furthermore since the effective potential is written as an expansion in powers of a/T we need that this ratio is not too much larger than 1 (there are numerical factors in Eq. (13) that make it possible to consider values for a/T_c slightly larger than 1). From Eqs. (15) and (16) the coupling constants are proportional to m_σ which, from the above conditions, restricts the analysis to considering not too large values of m_σ. Since the purpose of this work is not to pursue a precise determination of the couplings but instead to call attention to the fact that the proper treatment of screening effects allows the linear sigma model to provide solutions for the CEP, we consider small values for m_σ. The Particle Data Group quotes 400 MeV $\leq m_\sigma \leq$ 550 MeV [31]. There are also analyses that place m_σ close to the two-pion threshold [32]. Given that σ is anyhow a broad resonance, in order to satisfy the above requirements let us first take for definitiveness two values $m_\sigma = 300$ and 400 MeV, namely, close to the two-pion threshold. Therefore, the allowed values for the couplings λ and g are restricted by

$$\sqrt{\frac{\lambda}{2} + \frac{N_f N_c g^2}{6}} = 0.77\ ,\ 1.28. \tag{17}$$

Eq. (17) provides a relation between λ and g. A possible solution consistent with the above requirements is given by $\lambda = 0.2$, $g = 0.71$ for $m_\sigma = 300$ MeV and by $\lambda = 0.86$, $g = 1.1$ for $m_\sigma = 400$ MeV.

Figs. 1 and 2 show the phase diagram obtained for the sets of allowed values λ and g for $m_\sigma = 300, 400$ MeV. Note that for small μ the phase transition is second order. In this case the (pseudo)critical temperature is determined from setting the second derivative of the effective potential in Eq. (13) to zero at $v = 0$. When μ increases, the phase transition becomes first order. The critical temperature is now computed by looking for the temperature where a secondary

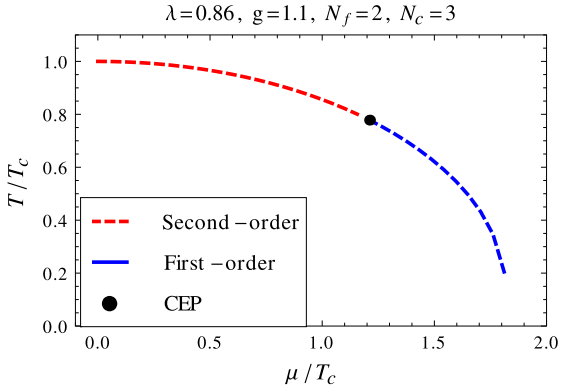

Fig. 2. Effective QCD phase diagram computed for $\lambda = 0.86$ and $g = 1.1$ obtained by considering $m_\sigma^{\text{vac}} = 400$ MeV. For small values of μ the phase transition is of second order. The order of the transition changes to first order for larger values of μ. The CEP is located at $(\mu^{\text{CEP}}/T_c, T^{\text{CEP}}/T_c) \sim (1.2, 0.8)$.

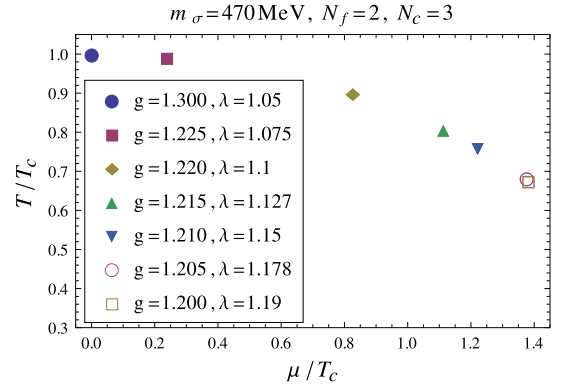

Fig. 3. CEP's location for $m_\sigma = 470$ MeV for different values of λ and g, with the condition $g > \lambda$ and consistent with Eq. (15).

minimum for $v \neq 0$ is degenerate with a minimum at $v = 0$. In both of these cases, from the detailed analysis, we locate the position of the CEP as $(\mu^{\text{CEP}}/T_c, T^{\text{CEP}}/T_c) \sim (1.2, 0.8)$, which is in the same range as the CEP found from lattice inspired analyses [9]. Note also that the phase transition curve is essentially flat close to the T axis which goes also in line with the results of Ref. [33].

Fig. 3 shows the location of the CEP for $m_\sigma = 470$ MeV (which is at the upper edge for the values allowed in our approach) when varying λ and g according to Eq. (15) with the condition $g > \lambda$. We observe that a small difference between λ and g favors a CEP's location away from the vertical axis and that when the difference between the couplings increases, the CEP moves toward the T axis. We can understand this behavior by noticing that since g controls the strength of the fermion's contribution to the effective potential and that the first-order nature of the transition is governed by these particles, when λ and g are similar, the first-order phase transition starts for larger values of μ. When this difference increases, the fermion contribution to the effective potential is important to start with and thus the first-order transitions start for smaller values

of μ. Also note that although the CEP's location shows a large dispersion, we still find solutions consistent with the location obtained for the other two explored values of m_σ.

We thus see that the allowed values for the couplings are not uniquely determined. In order to discriminate between different sets of couplings and further constrain their values, one could resort to study another observable such as the pressure. As shown by lattice QCD [34], this quantity is a monotonically increasing function of temperature. We have performed preliminary studies that show that there are sets, among the explored ones, that satisfy this behavior for the pressure. A more detailed analysis focusing on this observable is on its way and will be reported elsewhere. Nevertheless, we point out that in order to have access to a more precise determination of the couplings, the model needs first to be refined to either include higher powers of a/T in the analysis or to allow a description for the case with $a/T > 1$.

In conclusion, we have shown that it is possible to obtain values for the couplings that allow to locate the CEP in the region found by mathematical extensions of lattice analyses. Since the linear sigma model does not have confinement we attribute this location to the adequate description of the plasma screening properties for the chiral symmetry breaking at finite temperature and density. These properties are included into the calculation of the effective potential through the boson's self-energy and in the determination of the allowed range for the coupling constants through the observation that the thermal boson masses vanish at the phase transition for $\mu = 0$. These observations determine a relation between the model parameters which is put in quantitative terms by taking physical values for T_c from lattice calculations and for a from the vacuum boson masses. We believe this description will play an important role in determining the location of the CEP also in QCD.

Acknowledgements

A.A. acknowledges useful comments from M.E. Tejeda-Yeomans, M. Loewe and A.J. Mizher. J.J. Cobos-Martínez acknowledges support from a CONACyT-México postdoctoral fellowship under contract number 290917-UMSNH. Support for this work has been received in part from UNAM-DGAPA-PAPIIT grant number 101515, from CONACyT-México grant number 128534 and from CIC-UMSNH grant numbers 4.10 and 4.22.

References

[1] Y. Aoki, G. Endrődi, Z. Fodor, S.K. Katz, K.K. Szabó, Nature 443 (2006) 675.
[2] L. Levkova, PoS Lattice 2011 (2011) 011.
[3] C. Bernard, et al., MILC Collaboration, Phys. Rev. D 71 (2005) 034504.
[4] M. Cheng, et al., Phys. Rev. D 74 (2006) 054507.
[5] S. Borsányi, et al., J. High Energy Phys. 1009 (073) (2010);
Y. Aoki, et al., J. High Energy Phys. 0906 (088) (2009);
Y. Aoki, et al., Phys. Lett. B 643 (2006) 46.
[6] A. Bazavov, PoS Lattice 2011 (2011) 182;
A. Bazavov, et al., Phys. Rev. D 85 (2012) 054503.
[7] T. Bhattacharya, et al., Phys. Rev. Lett. 113 (2014) 082001.
[8] P. de Forcrand, PoS Lattice 2009 (2009) 010.
[9] Z. Fodor, S.D. Katz, J. High Energy Phys. 0203 (2002) 014;
A. Li, A. Alexandru, X. Meng, K.F. Liu, Nucl. Phys. A 830 (2009) 633C;
P. de Forcrand, S. Kratochvila, Nucl. Phys. B, Proc. Suppl. 153 (2006) 62.
[10] S.-x. Qin, L. Chang, H. Chen, Y.-x. Liu, C.D. Roberts, Phys. Rev. Lett. 106 (2011) 172301;
C.S. Fischer, J. Luecker, Phys. Lett. B 718 (2013) 1036;
C. Shi, Y.-L. Wang, Y. Jiang, Z.-F. Cui, H.-S. Zong, J. High Energy Phys. 1407 (2014) 014;

E. Gutiérrez, A. Ahmad, A. Ayala, A. Bashir, A. Raya, J. Phys. G 41 (2014) 075002.
[11] M. Asakawa, K. Yazaki, Nucl. Phys. A 504 (1989) 668;
A. Barducci, R. Casalbuoni, S. De Curtis, R. Gatto, G. Pettini, Phys. Lett. B 231 (1989) 463;
Phys. Rev. D 41 (1990) 1610;
A. Barducci, R. Casalbuoni, G. Pettini, R. Gatto, Phys. Rev. D 49 (1994) 426;
J. Berges, K. Rajagopal, Nucl. Phys. B 538 (1999) 215;
M.A. Halasz, A.D. Jackson, R.E. Shrock, M.A. Stephanov, J.J.M. Verbaarschot, Phys. Rev. D 58 (1998) 096007;
O. Scavenius, A. Mocsy, I.N. Mishustin, D.H. Rischke, Phys. Rev. C 64 (2001) 045202;
N.G. Antoniou, A.S. Kapoyannis, Phys. Lett. B 563 (2003) 165;
Y. Hatta, T. Ikeda, Phys. Rev. D 67 (2003) 014028.
[12] S. Sharma, Adv. High Energy Phys. 2013 (2013) 452978.
[13] C. Sasaki, B. Friman, K. Redlich, Phys. Rev. D 77 (2008) 034024;
P. Costa, M.C. Ruivo, C.A. de Sousa, Phys. Rev. D 77 (2008) 096001.
[14] W.-j. Fu, Z. Zhang, Y.-x. Liu, Phys. Rev. D 77 (2008) 014006;
H. Abuki, R. Anglani, R. Gatto, G. Nardulli, M. Ruggieri, Phys. Rev. D 78 (2008) 034034;
B.J. Schaefer, M. Wagner, Phys. Rev. D 79 (2009) 014018;
P. Costa, H. Hansen, M.C. Ruivo, C.A. de Sousa, Phys. Rev. D 81 (2010) 016007.
[15] P. Kovács, Z. Szép, Phys. Rev. D 77 (2008) 065016.
[16] B.J. Schaefer, J.M. Pawlowski, J. Wambach, Phys. Rev. D 76 (2007) 074023.
[17] M. Loewe, F. Marquez, C. Villavicencio, Phys. Rev. D 88 (2013) 056004;
G. Gomez Dumm, Braz. J. Phys. 38 (2008) 396.
[18] G.S. Bali, F. Bruckmann, G. Endrodi, Z. Fodor, S.D. Katz, S. Krieg, A. Schafer, K.K. Szabo, J. High Energy Phys. 02 (2012) 044.
[19] G.S. Bali, F. Bruckmann, G. Endrodi, Z. Fodor, S.D. Katz, A. Schafer, Phys. Rev. D 86 (2012) 071502.
[20] G.S. Bali, F. Bruckmann, G. Endrodi, S.D. Katz, A. Schafer, J. High Energy Phys. 08 (2014) 177.
[21] A. Ayala, M. Loewe, A.J. Mizher, R. Zamora, Phys. Rev. D 90 (2014) 036001.
[22] A. Ayala, M. Loewe, R. Zamora, Phys. Rev. D 91 (2015) 016002.
[23] L. Dolan, R. Jackiw, Phys. Rev. D 9 (1974) 3320.
[24] M.E. Carrington, Phys. Rev. D 45 (1992) 2933.
[25] A. Ayala, J.J. Cobos-Martinez, M. Loewe, M.E. Tejeda-Yeomans, R. Zamora, Phys. Rev. D 91 (2015) 016007.
[26] See for example E.S. Bowman, J.I. Kapusta, Phys. Rev. C 79 (2009) 015202;
D. Kroff, E.S. Fraga, arXiv:1409.7026 [hep-ph].
[27] See for example C.S. Fischer, J. Luecker, C.A. Welzbacher, Phys. Rev. D 90 (2014) 034022;
C.S. Fischer, J. Luecker, Phys. Lett. B 718 (2013) 1036;
C.S. Fischer, J. Luecker, J.A. Mueller, Phys. Lett. B 702 (2011) 438;
A. Ayala, A. Bashir, C.A. Dominguez, E. Gutierrez, M. Loewe, A. Raya, Phys. Rev. D 84 (2011) 056004.
[28] A. Ayala, A. Bashir, A. Raya, A. Sánchez, Phys. Rev. D 80 (2009) 036005.
[29] A. Ayala, L.A. Hernández, A.J. Mizher, J.C. Rojas, C. Villavicencio, Phys. Rev. D 89 (11) (2009) 116017.
[30] Y. Maezawa, S. Aoki, S. Ejiri, T. Hatsuda, N. Ishii, K. Kanaya, N. Ukita, J. Phys. G 34 (2007) S651.
[31] Particle Data Group, http://pdg.lbl.gov.
[32] See for example V.V. Anisovich, Int. J. Mod. Phys. A 21 (2006) 3615.
[33] G. Endrodi, Z. Fodor, S.D. Katz, K.K. Szabo, J. High Energy Phys. 1104 (2011) 001.
[34] S. Borsanyi, Z. Fodor, C. Hoelbling, S.D. Katz, S. Krieg, C. Ratti, K.K. Szabo, arXiv:1410.7917 [hep-lat].